

# Unusual polarization patterns in flat epitaxial ferroelectric nanoparticles

Ivan I. Naumov and Alexander M. Bratkovsky

Hewlett-Packard Laboratories, 1501 Page Mill Road, Palo Alto, California 94304

(Dated: February 10, 2022)

PACS numbers: 77.80.Bh, 77.22.Ej, 77.84.Dy

Interest in epitaxial ferroelectric nanoislands was growing rapidly in recent years driven by their potential for devices, especially ultradense memories [1, 2, 3, 4]. Recent advances in the “bottom-up” (self-assembly) nanometer scale techniques have opened up the opportunities of fabricating high-quality epitaxial ferroelectric nanoislands with extremely small thickness and lateral size on the order of 1 nm and 20 nm, respectively [4, 5, 6, 7, 8]. On the other hand, recent emergence of powerful probes, such as piezoresponse force microscopy (PFM), has enabled imaging of a local domain structure with sub-10 nm resolution [3, 9, 10]. In spite of those developments, a clear understanding of the polarization patterns in epitaxial ferroelectric nanoislands is lacking, and some important characteristics, like a critical lateral size for ferroelectricity, are not yet established. Here, we perform *ab-initio* studies of non-electroded epitaxial  $\text{Pb}(\text{Zr}_{0.5}\text{Ti}_{0.5})\text{O}_3$  (PZT) and  $\text{BaTiO}_3$  (BTO) nanoislands and show the existence of novel polarization patterns driven by the misfit strains and/or anisotropy energy. The results allow interpretation of the data and design of the ferroelectric nanostructures with tailored response to external field.

Geometrically, nanoislands or flat nanoparticles represent a class of systems that bridge the gap between 0D nanodots and 2D ultra-thin films. Compared with thin films, they have free-standing side walls that tend to suppress the formation of uniform in-plane polarization because of appearing depolarizing field, like in ferroelectric [11, 12] or ferromagnetic particles [13]. On the other hand, relative to the (confined in all three dimensions) nanodots, they have large aspect ratio and likely to behave similarly to thin films when the polarization is out-of-plane. These observations lead one to expect that ferroelectric nanoislands should exhibit some kind of a “particle-to-thin film” crossover behavior and related novel effects depending on the aspect ratio and the type of bulk polarization ordering (which is different in PZT compared to BTO crystals).

Free-standing ferroelectric nanodots usually lose stability with respect to a vortex ground state, in which the polarization curls around some vortex core(s). Such an ordering can be characterized, in simplest single vortex cases, by a *toroidal* moment or a moment of polarization [14, 15, 16, 17]. This is analogous, to some extent, to the

magnetic vortices in magnetic particles [13], but there are also qualitative differences due to electrostatic interactions and inhomogeneity energy in ferroelectric particles being larger than the magnetic analogues by many orders of magnitude. Note also that the symmetry of the bulk cubic crystals of BTO or PZT does not allow for a “bulk” toroidal moment [18], such an ordering in the present case is entirely due to presence of boundaries of the particles and the accompanying it depolarizing/demagnetizing field. The moment of polarization appears continuously at the critical point and may be regarded as an order parameter for such a transition in an island [14].

We shall consider below the nanoislands of cubic perovskite materials. The epitaxial thin films of such materials become uniaxial under compressive strain with an easy axis perpendicular to the film, and usually form a  $180^\circ$  stripe (c-)domain structure [19, 20, 21, 22, 23, 24, 25, 26, 27, 28]. One can, therefore, anticipate the flat ferroelectric nanoislands with large aspect ratio to undergo an unusual vortex to stripe domains transformation with an increasing compressive misfit strain. We show below that perovskite nanoislands do indeed undergo such a transition, but only via one or two *intermediate* phases where in-plane curling polarization coexist with the  $180^\circ$  c-domains. Moreover, the domain phase does not necessarily render the well known  $180^\circ$  stripe domain structure, but also can take the form of a  $180^\circ$  *tweed texture*, depending on the anisotropy energy. We also demonstrate that stripe and tweed textures evolve differently in applied external electric field.

The simulated nanoparticles have circular and/or rectangular shapes and the following dimensions:  $19 \times 6$ ,  $39 \times 10$  for the former and  $39 \times 39 \times 10$  for the latter (all dimensions are given in lattice parameters of the cubic bulk phase  $a$ , which is  $4.00\text{\AA}$  and  $3.95\text{\AA}$  for PZT and BTO, respectively). The  $z$ -axis is selected along the (shortest) pseudocubic [001] direction normal to the substrate. To simulate finite-temperature behavior of the particles, we use the effective Hamiltonian

$$H\{\mathbf{u}_i\} = H^b\{\mathbf{u}_i\} + H^s\{\mathbf{u}_i\} - \sum_i Z^* \mathbf{u}_i \cdot \mathbf{E}_0, \quad (1)$$

whose primary variable is  $\mathbf{u}_i$ , the local soft mode in the unit cell  $i$  [29, 30]. The first part of the Hamiltonian,  $H^b$  is the same as in infinite bulk materials: its first-principles-derived parameters for BTO are given in [29], and for PZT- in [30]. The second part,  $H^s$ , represents the corrections to the  $H^b$  associated with the presence

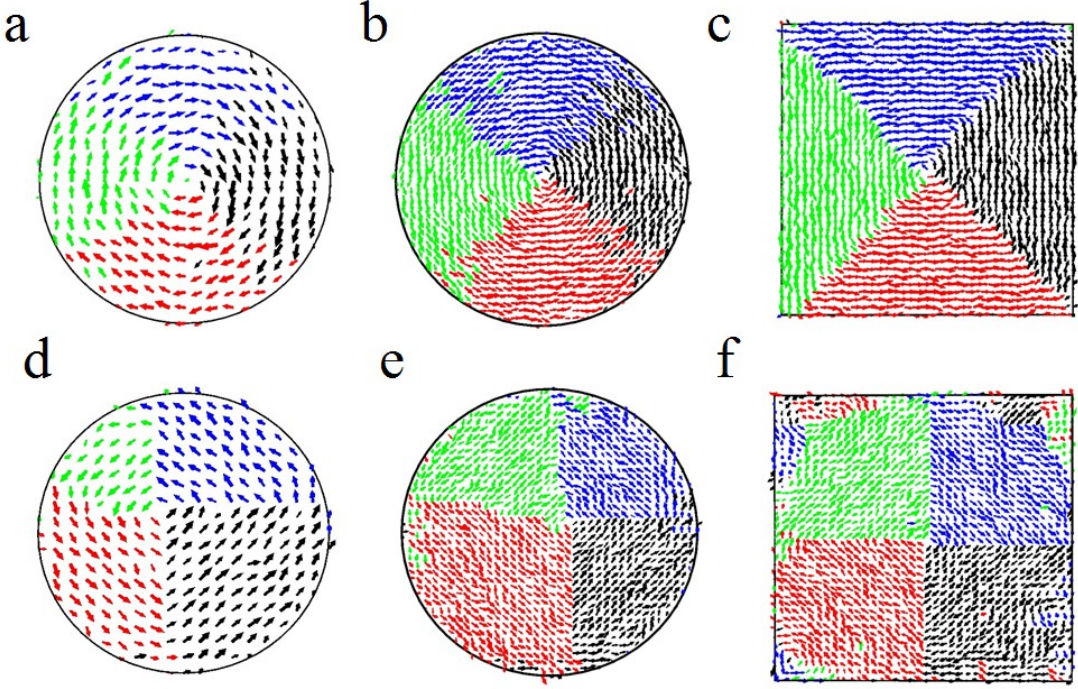


FIG. 1: Low-temperature polarization distributions on the central  $z$ -plane in PZT (a,b,c) and BTO (d,e,f) nanoparticles in free-standing states. (a,d)–  $19 \times 6$  nanodisks, (b,e)–  $39 \times 10$  nanodisks and (c,f)–  $39 \times 39 \times 10$  particles with square footprints. Shown in red, blue, green and black are the dipoles directed predominantly along  $[\pm 100]$  and  $[0 \pm 10]$  in PZT and along  $[\pm 1 \pm 10]$  in BTO systems.

of free surface via “vacuum-local mode” and “vacuum-inhomogeneous strain” interactions [31, 32]. And, finally, the third term describes the interaction of the local site dipoles  $\mathbf{p}_i = Z^* \mathbf{u}_i$  with an external field  $\mathbf{E}_0$  [33] ( $Z^*$  is the effective Born charge of the local mode  $\mathbf{u}_i$ ). We should stress that the first-principles-derived Hamiltonian is able to reproduce some nontrivial properties beyond the properties it was fit to: phase diagram, occurrence of an exotic monoclinic phase in a small range of Ti concentrations in bulk PZT, stripe c-domains in thin films with compressive in-plane strains, etc. Typically, 40,000 Monte Carlo sweeps are used to find the equilibrium dipole configuration at a fixed temperature. Open-circuit boundary conditions are assumed, so that no screening charges are taken into consideration. The effect of a substrate is imposed by fixing the homogeneous in-plane strain in the whole island:  $\epsilon_{xx} = \epsilon_{yy} = \epsilon$ ,  $\epsilon_{xy} = 0$ .

Our calculations predict that at low temperatures and in free-standing states all the investigated nanoparticles transform into a vortex ground state characterized by a nonzero toroidal moment  $\mathbf{G} = (2N)^{-1} \sum_i \mathbf{r}_i \times \mathbf{p}_i$ , where  $N$  is the total number of unit cells. In disk-shaped PZT particles (Fig. 1a,b), the local dipoles rotate from cell to cell forming the classical vortex patterns. But in a rectangular PZT  $39 \times 39 \times 10$  particle the polarization aligns with the square boundary as much as possible, hence the discontinuity lines (domain walls) form, and the resulting

pattern can be viewed as consisting of four domains separated by  $90^\circ$  domain walls (Fig. 1c). This is in a clear analogy with ordering in magnetic particles [13], anticipated for ferroelectric particles back in 1950s [11, 12]. The polarization in each domain point along one of the four pseudocubic  $[\pm 100]$  and  $[0 \pm 10]$  directions, so that the domain walls are parallel to the  $(1 \pm 10)$  crystallographic planes and pass through the center of the particle. In BTO particles, regardless of their shape and size, the dipoles tend to be directed along the  $[\pm 1 \pm 10]$  directions (Fig. 1d,e,f). As a result, two  $(100)$ -type  $90^\circ$  domain walls are likely to be formed crossing each other at the geometric center of the particles. The walls are rather fuzzy in bigger particles, especially in a rectangular  $39 \times 39 \times 10$  dot where the dipoles are frustrated near the lateral surfaces.

The different behavior of PZT and BTO free-standing nanoparticles can be easily understood by looking at the anisotropy energy  $\sum_i \gamma_i (u_{ix}^2 u_{iy}^2 + u_{ix}^2 u_{iz}^2 + u_{iy}^2 u_{iz}^2)$  in the effective Hamiltonian  $H$  (its part  $H^b$ ). Suppose that the amplitude  $|u|$  is fixed, then the anisotropy energy will approach its minimum either for  $\mathbf{u}$  along the  $[100]$  direction ( $\gamma > 0$ ) or along the  $[111]$  direction ( $\gamma < 0$ ). For PZT, the parameter  $\gamma$  (associated with the dominating Ti-centered unit cells) is positive [30] – this is consistent with the fact that PZT in bulk form adopts a tetragonal structure with an “easy” direction of polarization along  $[100]$ . At the same time, in BTO  $\gamma < 0$  [29], and this

system in bulk has a rhombohedral equilibrium structure with easy direction [111] and the equivalent bulk diagonals. Let us compare now, for example, two  $39 \times 39 \times 10$  PZT and BTO particles. In both cases, the effects of depolarizing field force the dipoles to lie in the  $x, y$ -plane. In the case of the PZT particle, however, the materials anisotropy factor is in compliance with the shape: majority of the dipoles are oriented along the easy directions [100] and [010] and at the same time they are parallel to the surface. The situation is quite different for the BTO particles, where *none* of the dipoles can be directed along the easy [111] body diagonal: in this case the majority of dipoles in the center region prefer to be oriented along [110] instead of the [111] direction. Near the side surfaces, however, the depolarizing field forces the dipoles to align with the square geometry, which increases the anisotropy energy term. The competition between these forces leads to the dipole frustration near the vertical walls and to the formation of four additional vortices near the corners (Fig. 1f) in agreement with the previous calculations for a  $24 \times 24 \times 24$  BTO nanodot [31].

The tensile strains stabilize the vortex states further, as seen from Fig. 2, increasing the  $z$ -component of the toroidal moment. On the contrary, compressive strains enhance the out-of-plane polarization, decrease  $G_z$  and eventually lead, as analysis below shows, to a  $180^\circ$  multi-domain structure running through the entire thickness of the islands. It is remarkable that in the case of BTO particles the critical strain associated with this transition is very small, approximately zero,  $\approx 0\%$ . In the PZT case, the critical strain dramatically decreases from 1.2 % to  $\approx 0\%$  when one increases the diameter from 19 to 39. The bigger PZT particle in a vortex state can tolerate the compressive strains less because its optimal in-plane averaged lattice parameter is noticeably larger than that corresponding to the bulk cubic phase (Fig. 2b).

In the PZT nanoparticles, the  $180^\circ$  multi-domain phase is nothing but the well-known  $180^\circ$  stripe domain structure found previously in infinite PZT thin films [25, 27]. Here, like in the thin films, the “up” and “down” domain run along [100] and alternate along [010] direction (Fig. 3a,b). The domain width, however, is not homogeneous across the particles: it is larger in the interior region and becomes 1-2 unit cell narrower near the edge of the particles. Besides, the stripes become wider in bigger particles. In a circular  $6 \times 19$  particle, for example, the width of the central stripe is 4 unit cells (16 Å), while it is 6 unit cells (24 Å) in  $10 \times 39$  and  $10 \times 39 \times 39$  particles. In both cases the stripes are narrower than that found in the PZT thin film modeled with a  $40 \times 40 \times 5$  supercell (8 unit cells), despite the fact that our particles are thicker.

BTO nanoparticles, in comparison with PZT counterparts, adopt not straight, but curved zig-zag-type stripes, running predominantly in [110] and  $[1-10]$  directions (Fig. 3c,d). Though rarely, they intersect each other forming a  $180^\circ$  tweed domain texture, which is drastically different from that found in BTO thin films [20, 28]. In the case of thin films, the stripes run only along one di-

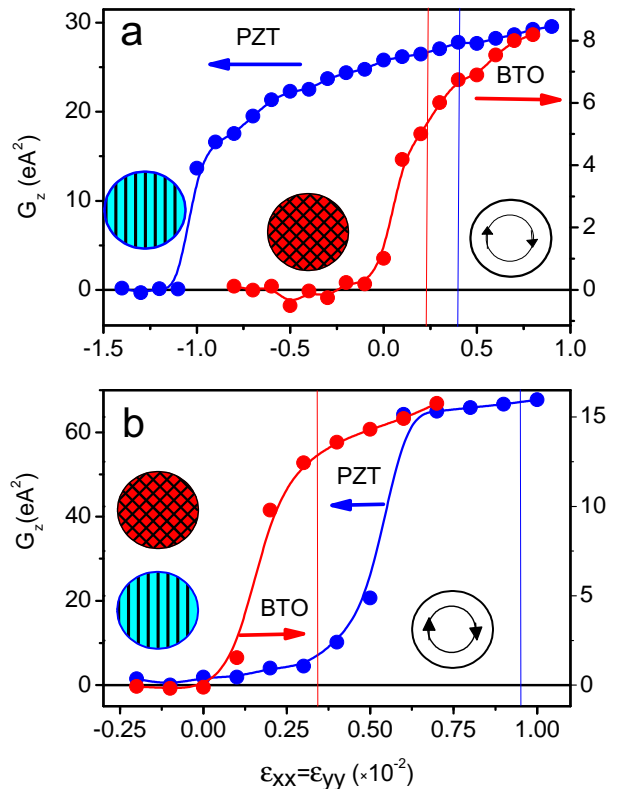


FIG. 2: The  $z$ -component of the toroidal moment as a function of strain in  $19 \times 6$  (a) and  $39 \times 10$  (b) nanoparticles. The strains are measured relative to the theoretical LDA-calculated lattice constants in bulk cubic structures. Note that in free standing states the particles are characterized by non-zero “residual” strains marked by vertical lines. The residual strain increases in passing from  $19 \times 6$  to  $39 \times 10$  systems, especially in PZT.

rection (either [110] or  $[1-10]$ ) and the system loses its four-fold symmetry axis perpendicular to the film. In the nanoparticles, however, the axis of the 4-th order is (on average) preserved by allowing the forming stripes to propagate in both possible directions. The stripes width changes from place to place, being less than 4 lattice constants on average. This value can be compared with 4.3 lattice periods found in BTO thin films [28].

As the present analysis shows, the transformation “vortex-to- $180^\circ$  domains” does not occur directly, but rather via one or even two intermediate structures. The simplest case is presented by a  $19 \times 6$  PZT particle having only a single intermediate structure. This structure develops from the vortex core that turns out to be longitudinally polarized already in a free-standing state. While the core region (with the radius 3-4 lattice spacings) embraces the polarization pointing “up”, beyond this radius the polarization tilts weakly out of plane oppositely to the core region, so that sum of all the dipoles add up to zero (Fig. 4). Under compressive strains, the vortex core ra-



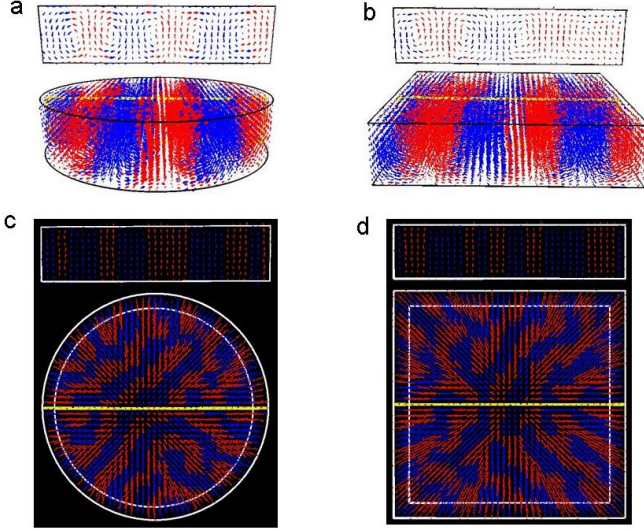


FIG. 3: Low-temperature three-dimensional polarization patterns in free-standing (001) PZT (a,b) and BTO (c,d) nanoparticles under compressive strain of -2%. (a,c)– 39×10 nanodisks, (b,d)– 39×39×10 particles with square footprints. The small rectangular inserts show the cross sections of a central vertical plane indicated by yellow lines. Red and blue arrows show local dipoles with positive and negative  $z$ -component, respectively.

dius expands and becomes comparable to the lateral size of the particles. At this stage, the  $x, y$ -components of the local dipoles still form a vortex, while the out-of-plane component,  $z$ , breaks the system into coaxially oppositely polarized cylindrically symmetric domains–skyrmion-like structure [34]. As the compressive strain further increases, this structure abruptly transforms into a  $180^\circ$  stripe domain phase with zero moment  $G$  (Fig. 2a).

In all other particles (both PZT and BTO), the structural transformation into  $180^\circ$  domain phase occurs in a two-step fashion. At first and relatively short stage, again, two symmetry conforming  $180^\circ$  coaxial domains develop at the expense of the toroidal moment (skyrmion structure). As the in-plane compression increases, this skyrmion structure transforms into  $180^\circ$  stripe (tweed) domains, as demonstrated in Fig. 5 for a 39×10 PZT nanoparticle. Remarkably, this happens on the background of nonzero  $G_z$ . And finally, the toroidal moment disappears at a critical compressive strain, and the system enters into a pure stripe or tweed domain phase.

If the compressive strains are released, the system in a  $180^\circ$  domain state relaxes back to a vortex dipole configuration. Typical evolution of the toroidal moment and the average value of the  $z$ -component of the local mode  $|u_z| = N^{-1} \sum_i |u_{i,z}|$  with the number of the Monte-Carlo sweeps is shown in Fig. 6. It is seen that the  $G_z$  component first linearly and then non-linearly increases, until saturation is reached, the other two components being practically null. The  $|u_z|$ , which is simply proportional

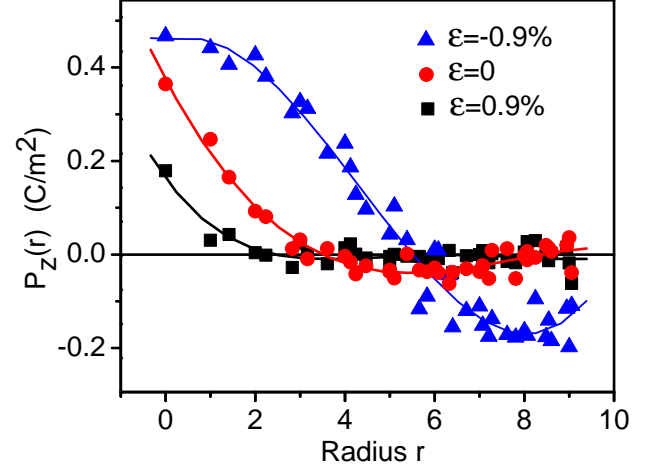


FIG. 4: Vertical polarization component in a 19×6 PZT disk at different misfit strains. While the values are radially averaged, they correspond to an instant moment of time and represent the fluctuating dipole structure. The lines represent 4-th order polynomial fits to the instant polarizations.

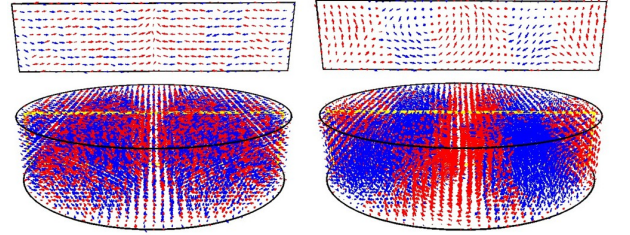


FIG. 5: Distribution of polarization in a 39×10 PZT nanodisk for two close strains of 0.6 % (left) and 0.5 % (right). The latter, which is more compressive relative to the free standing nanoparticle, leads to a state where  $180^\circ$  domains coexist with the curling polarization. The small rectangular inserts show the cross sections of a central vertical plane indicated by yellow lines. Red and blue arrows show local dipoles with positive and negative  $z$ -component, respectively.

to the average magnitude of the out-of-plane polarization  $|P_z|$ , decreases in a similar way, until it becomes saturated at some non-zero value. The last fact is mainly connected with the oppositely polarized core (“up”) and periphery region (“down”).

Consider now how the stripe domain and tweed structures evolve under the external electric field. The typical behavior of PZT systems is presented by a cylindrical particle 10×39, whose evolution under different fields applying along  $z$  is shown in Fig. 7. One can see that the dipoles with the direction opposite to the applied field start flipping first near the particle edge. When the field is further increased, the “switching front” propagates to the center, shrinking the length of the stripes and (to a lesser extent) their width, still being opposite to the field.

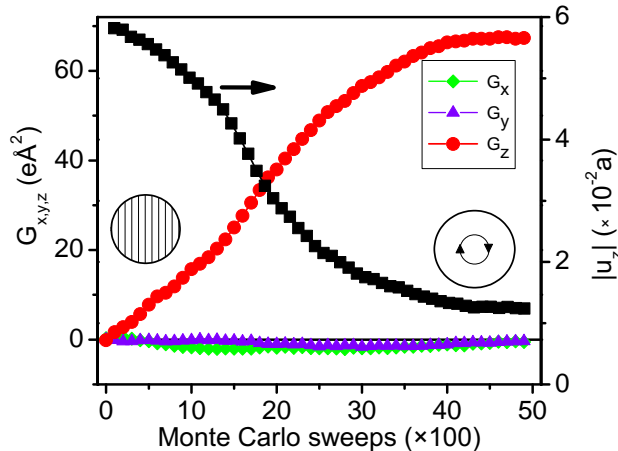


FIG. 6: The evolution of the toroidal moment  $\mathbf{G}$  and average magnitude of the z-component of the local mode in a  $39 \times 10$  PZT disk after “switching” off compressive strains.

Ultimately, one reaches a state in which only one reduced stripe remains, near the particle center; this stripe has an elliptical cross section and can be called a “bubble” (Fig. 7,  $E = 50 \times 10^6$  V/cm). BTO nanoparticles behave qualitatively similar to the PZT counterparts only in the initial stage of evolution: there the dipoles also start flipping in the field direction in the rim region causing the longitudinal shrinking of the stripes. Now, however, the stripe shrinking is accompanied by their breaking into pieces (substripes) which, in turn, transform into nanobubbles. As a result, several relatively thin bubbles form near the center before the systems enters a monodomain state (Fig. 7,  $40 \times 10^6$  V/cm). Note that both in PZT and BTO, the out-of-plane polarization linearly increases with the electric field, similar to the case of ultra-thin films [27, 28].

All the considered above intermediate phases (including skyrmion-like) are characterized by z-domains coexisting with the in-plane curling polarization; they can be called the “domain-patterned vortex” structures. Interestingly, such structures have never been reported for ferroelectric small systems, though has been found in flat magnetic particles with low perpendicular anisotropy [35]. Analogously, the  $180^\circ$  tweed domain texture has never been discovered in ferroelectric nanostructures, though resembles pretty much the labyrinthine phase observed in ultrathin magnetic films [36]. One can think that this structure is metastable and eventually will evolve into an ordinary stripe phase. In our simulations, however, we did not observe any signs of such transitions even after a huge running time, more than 500 000 Monte Carlo sweeps.

Our predictions can be helpful for understanding some puzzling and controversial experimental results [5, 6, 7, 8]. While the authors [5, 7] did not observe any piezore-

sponse of the  $\text{PbTiO}_3$  islands with the diameters smaller than 20 nm, Ref. [6] reported observation of ferroelectricity in zirconate titanate nanoparticles with the lateral size as small as 9 nm. On the other hand, according to measurements [8], the relationship between the size of nanoislands and occurrence of ferroelectricity is rather random, raising the question why some particles are ferroelectric, but the other (even with very similar sizes) are not. Based on our results, we can explain these uncertainties in the experimental results in the following way. As compared with continuous thin films, the existence of free side walls in nanoislands leads to new and additional mechanisms of the strain relaxations [37], including formation of partial or full misfit dislocations at nodes of the lateral surfaces and the flat plane of the substrate. This implies that with the shrinking in lateral size, the maintaining of coherent mismatch lattice strains in a nanoisland becomes more and more difficult, and it is very likely that under the same experimental conditions the smaller particles will experience less external strains. Moreover, since the magnitude of strains is not well-controlled, even the particles with comparable sizes can be differently strained. But in this case, according to our calculations, they can show totally different piezoresponses. Indeed, as the compressive strain is relaxed, an island can transform into an intermediate or even in a vortex state, which is unable to produce any (vertical or lateral) PFM signal at all. The particle in a vortex state should be viewed as a paraelectric one showing only linear and hysteresis-free piezoresponse as a function of dc bias voltage applied to the AFM tip. Similar arguments can be used in interpretation the results of Ref. [38] reporting the absence of the local piezoresponse loop in a PZT nanoisland with a height of 10 nm [38]. Although the authors attributed this effect to the inhomogeneous elastic fields associated with misfit dislocations [38], it also can be explained by the formation of a curling polarization.

In summary, we investigate the strain effects on (001)-epitaxial PZT and BTO nanoislands using first-principle-derived effective Hamiltonian approach. Our study leads to the following conclusions: (i) regardless of size, shape, and material, all the investigated particles transform into a vortex state with in-plane curling polarization; the latter resembles classical vortex pattern in smaller/round particles, while in bigger/rectangular particles it can also be described as a domain structure with four closure domains and four  $90^\circ$  domain walls, (ii) under strong enough compressive strains the vortex state is no longer stable and yields to a  $180^\circ$  stripe domain phase in PZT and to a more symmetric,  $180^\circ$  tweed domain texture, in BTO nanoparticles, and (iii) these transitions proceed not directly, but via one or two *unusual* intermediate phases where domain structure coexist with circular vortex ordering. We further discovered that the electric-field induced evolution (switching) of multi-domain structures is essentially different for the two materials (PZT and BTO).

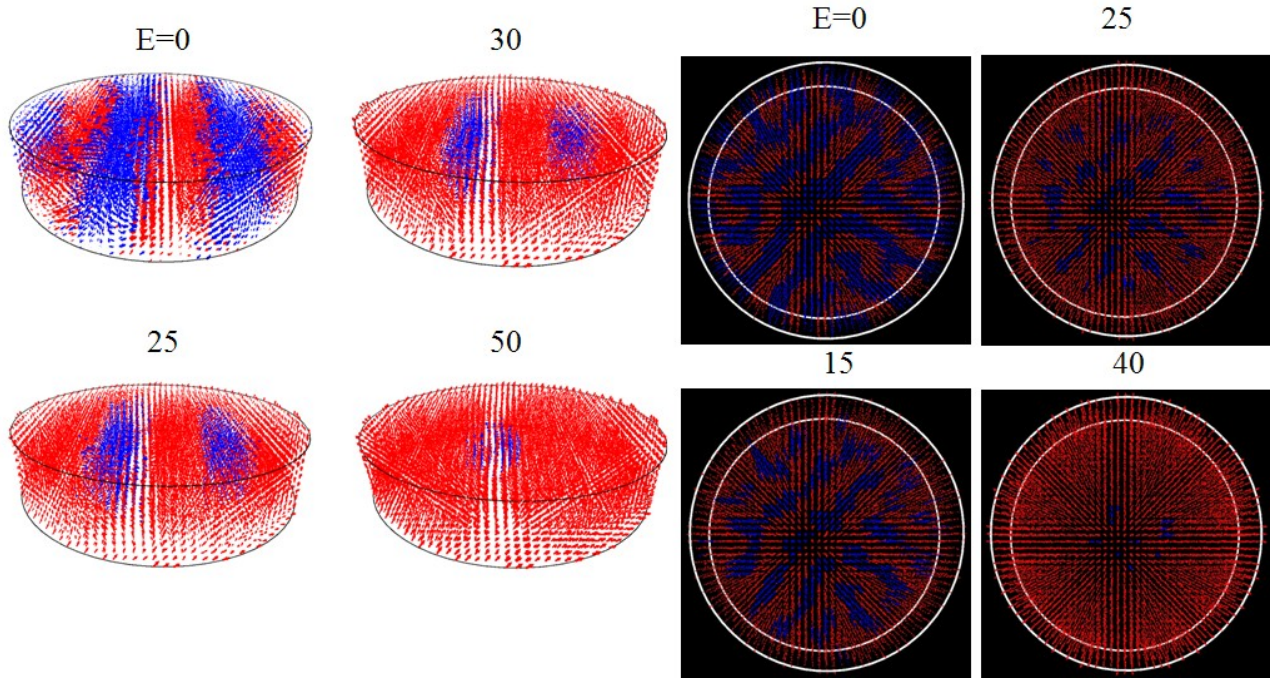


FIG. 7: Three-dimensional low-temperature polarization patterns in (001)  $39 \times 10$  PZT (white background) and BTO (black background) nanoparticles under compressive strain of  $-2\%$ , for different out-of-plane electric fields (in  $10^6$  V/cm).

- 
- [1] Scott, J. F. Application of modern ferroelectrics. *Science* **315**, 954-959 (2007).
  - [2] Lichtensteiger, C., Dawber, M., & Triscone, J.-M. Ferroelectric size effects. *Physics of Ferroelectrics: A Modern Perspective*, Topics Appl. Physics **105**, 305-337 (2007).
  - [3] Gruverman, A., & Kholkin, A. Nanoscale ferroelectrics: processing, characterization and future trends. *Rep. Prog. Phys.* **69**, 2443-2474 (2006).
  - [4] Alexe, M. & Hesse, D. Self-assembled nanoscale ferroelectrics. *J. Mater. Sci.* **41**, 1-11 (2006).
  - [5] Roelofs, A., Schneller, T., Szot, K. & Waser R. Towards the limit of ferroelectric grains. *Nanotechnology* **14**, 250-253 (2003).
  - [6] Seol, K. S., Takeuchi K. & Ohki Y. Ferroelectricity of single-crystalline, monodisperse lead zirconate titanate of 9 nm in diameter. *Appl. Phys. Lett.* **85**, 2325-2327 (2004).
  - [7] Okaniwa, M., Fujisawa, H., Shimizu, M., Niu H. & K. Honda. Piezo- and ferroelectric properties of self-assembled  $\text{PbTiO}_3$  nanosland structures fabricated by metalorganic chemical deposition. *Jpn. J. Appl. Phys.* **44**, 6891-6894 (2005).
  - [8] Shimizu, M., Nagata, M., Okaniwa, M., Fujisawa, H. & Osada, M. Size dependence of piezo- and ferroelectric properties of self-assembled  $\text{PbTiO}_3$  nanoslands fabricated by MOCVD. *Abs. of Int. Symp. on Integr. Ferroelectr.* (ISIF 2006), 4-380-C (Honolulu, Hawaii, USA, April 23-27, 2006).
  - [9] Alexe, M. & Gruverman, A. (Ed.). *Nanoscale Characterisation of Ferroelectric Materials: Scanning Probe Microscopy* (Springer, Berlin, 2004).
  - [10] Rüdiger, A. R. *et al.* Nanosize ferroelectric oxides— tracking down the superparaelectric limit. *Appl. Phys. Lett.* **80**, 1247-1255 (2005).
  - [11] Anliker, von M., Brugger H.R. & Kanzig, W. Das verhalten von kooloidalen seignetteelektrika III, bariumtitanat  $\text{BaTiO}_3$ . *Helv. Phys. Acta* **27**, 99-106 (1954).
  - [12] Kanzig, W. Wall energy of ferroelectric domains. *Phys. Rev.* **87**, 385 (1952).
  - [13] Hubert, A., & Schäfer, R. *Magnetic Domains: The Analysis of Magnetic Structures* (Springer, Berlin, 1998).
  - [14] Naumov, I., Bellaiche, L. & Fu, H. Unusual phase transitions in ferroelectric nanodisks and nanorods. *Nature (London)* **432**, 737-740 (2004).
  - [15] Ponomareva I., Naumov, I.I., Kornev, I., Fu, H. & Bellaiche, L. Atomistic treatment of depolarizing energy and field in ferroelectric nanostructures. *Phys. Rev. B* **72**, 140102 (R) (2005).
  - [16] Ponomareva I., Naumov, I.I. & Bellaiche, L. Low-dimensional ferroelectrics under different electrical and mechanical boundary conditions: Atomistic simulations. *Phys. Rev. B* **72**, 214118 (2005).
  - [17] Prosandeev, S. & Bellaiche, L. Characteristics and signatures of dipole vortices in ferroelectric nanodots: First-principles-based simulations and analytical expressions. *Phys. Rev. B* **75**, 094102 (2007).
  - [18] Gorbatshevich, A. A. & Kopaev, Yu. V. Toroidal order in crystals. *Ferroelectrics* **161**, 321-334 (1994).
  - [19] Bratkovsky, A. M. & Levanyuk, A.P. Abrupt appearance of the domain pattern and fatigue of thin ferroelectric films. *Phys. Rev. Lett.* **84**, 3177-3180 (2000); see also a review: arXiv/0801.1669v2 (2008).



- [20] Tinte, S. & Stachiotti, M. G. Surface effects and ferroelectric phase transitions in BaTiO<sub>3</sub> ultrathin films. *Phys. Rev. B* **64**, 235403 (2001).
- [21] Streiffer, S. K. *et al.* Observation of nanoscale 180 stripe domains in ferroelectric PbTiO<sub>3</sub> thin films *Phys. Rev. Lett.* **89**, 07601 (2002).
- [22] Fong, D. D. *et al.* Direct structural determination in ultrathin ferroelectric films by analysis of synchrotron x-ray scattering measurements. *Phys. Rev. B* **71**, 144112 (2005).
- [23] Fong, D. D. *et al.* Ferroelectricity in ultrathin perovskite films. *Science* **304**, 1650-1653 (2004).
- [24] Kornev, I., Fu, H. & Bellaiche, L. Ultrathin films of ferroelectric solid solutions under a residual depolarizing field. *Phys. Rev. Lett.* **93**, 196104 (2004).
- [25] Wu, Z. *et al.* Ferroelectricity in Pb(Zr<sub>0.5</sub>Ti<sub>0.5</sub>)O<sub>3</sub> thin films: Critical thickness and 180 stripe domains. *Phys. Rev. B* **70**, 104108 (2004).
- [26] Wu, Z. *et al.* Phase diagram of ultrathin Pb(Zr<sub>0.5</sub>Ti<sub>0.5</sub>)O<sub>3</sub> films under strain. *Appl. Phys. Lett.* **86**, 202903 (2004).
- [27] Lai, B.-K. *et al.* Electric-field-Induced domain evolution in ferroelectric ultrathin films. *Phys. Rev. Lett.* **96**, 137602 (2006).
- [28] Lai, B.-K., Ponomareva I., Kornev, I., Bellaiche, L. & Salamo, G. J. Domain evolution of BaTiO<sub>3</sub> ultrathin films under an electric field: A first-principles study. *Phys. Rev. B* **75**, 085412 (2007).
- [29] Zhong, W., Vanderbilt, D. & Rabe, K. M. First-principles theory of ferroelectric phase transitions for perovskites: The case of BaTiO<sub>3</sub> *Phys. Rev. B* **52**, 6301-6312 (1995).
- [30] Bellaiche, L., Garcia, A. & Vanderbilt, D. Finite-temperature properties of Pb(Zr<sub>1-x</sub>Ti<sub>x</sub>)O<sub>3</sub> alloys from first principles. *Phys. Rev. Lett.* **84**, 5427-5430 (2000); Low-temperature properties of Pb(Zr<sub>1-x</sub>Ti<sub>x</sub>)O<sub>3</sub> solid solutions. *Ferroelectrics* **266**, 41-56 (2002).
- [31] Fu, H. & Bellaiche, L. Ferroelectricity in barium titanate quantum dots and wires. *Phys. Rev. Lett.* **91**, 257601 (2003).
- [32] Almahmoud, E. *et al.* Properties of Pb(Zr,Ti)O<sub>3</sub> ultrathin films under stress-free and open-circuit electrical boundary conditions. *Phys. Rev. B* **70**, 220120(R) (2004).
- [33] Garcia, A. & Vanderbilt, D. Electromechanical behavior of BaTiO<sub>3</sub> from first principles. *Appl. Phys. Lett.* **72**, 2981-2983 (1998).
- [34] Röler, U. K., Bogdanov, A. N. & Pfleiderer, C. Spontaneous skyrmion ground states in magnetic metals. *Nature (London)* **442**, 797-801 (2006).
- [35] Maziewski, A., Zablotskii, V. & Kisielewski M. Geometry-driven out-of-plane magnetization states in nanostructures. *Phys. Rev. B* **73**, 134415 (2006).
- [36] Portmann, O., Vaterlaus, A. & D. Pesla D. An inverse transition of magnetic domain patterns in ultrathin films. *Nature (London)* **422**, 701-704 (2003).
- [37] Ovid'ko, L. A. Relaxation Mechanisms in Strained Nanoislands. *Phys. Rev. Lett.* **88**, 046103 (2002).
- [38] Chu, M.-W. *et al.* Impact of misfit dislocations on the polarization instability of epitaxial nanostructured ferroelectric perovskites. *Nature Materials* **3**, 87-90 (2004).